JOURNAL OF APPLIED PHYSICS **123**, 165104 (2018)

Effect of substrate rotation speed and off-center deposition on the structural, optical, and electrical properties of AZO thin films fabricated by DC magnetron sputtering

F. Turkoglu,[1,a)] H. Koseoglu,[1] S. Zeybek,[2] M. Ozdemir,[2] G. Aygun,[1] and L. Ozyuzer[1,2]
[1]*Department of Physics, Izmir Institute of Technology, 35430 Urla, Izmir, Turkey*
[2]*Teknoma Technological Materials Ltd., IZTEKGEB, IYTE Campus, Urla, Izmir, Turkey*

(Received 8 November 2017; accepted 7 April 2018; published online 24 April 2018)

In this study, aluminum-doped zinc oxide (AZO) thin films were deposited by DC magnetron sputtering at room temperature. The distance between the substrate and target axis, and substrate rotation speed were varied to get high quality AZO thin films. The influences of these deposition parameters on the structural, optical, and electrical properties of the fabricated films were investigated by X-ray diffraction (XRD), Raman spectroscopy, spectrophotometry, and four-point probe techniques. The overall analysis revealed that both sample position and substrate rotation speed are effective in changing the optical, structural, and electrical properties of the AZO thin films. We further observed that stress in the films can be significantly reduced by off-center deposition and rotating the sample holder during the deposition. An average transmittance above 85% in the visible range and a resistivity of $2.02 \times 10^{-3}\,\Omega$ cm were obtained for the AZO films. *Published by AIP Publishing.* https://doi.org/10.1063/1.5012883

I. INTRODUCTION

Transparent conducting oxides (TCOs) are commonly used as the front electrode for many microelectronic applications consisting of flat panel displays, light emitting diodes, and thin film solar cells because they have excellent transmittance in the visible wavelength and high electrical conductivity.[1,2] The function of the TCO layer in thin film solar cells is to allow all wavelengths beneath the cut-off wavelength to be transmitted to the absorber layer and allow electrical conduction to the contact grid.[3] Fluorine-doped tin oxide (FTO), indium-doped tin oxide (ITO), and highly doped ZnO, namely, with gallium (GZO), aluminum (AZO), or boron (BZO) are the most widely used TCO materials in thin film solar cells.[4] Among them, doped ZnO has gained a lot of attention owing to its advantages including low material cost, high band gap, non-toxic nature, and high transparency.[5,6] Particularly, among the ZnO-based materials, Al-doped ZnO (AZO) thin films are currently the most used materials for making transparent conducting electrodes because of their relatively low electrical resistivity and high optical transmittance.[7] Many deposition techniques such as pulsed laser deposition (PLD),[8] chemical vapor deposition,[9] and sputtering[10] can be employed for the deposition of AZO thin films. A high deposition temperature above 300 °C is necessary to get a desired TCO property in most of these methods since higher temperature provides an improvement in the crystallinity of the thin films.[11,12] On the other hand, higher temperature generates many defect states due to increased interfacial diffusion and results in a high charge carrier recombination rate.[11] Therefore, a room temperature (RT) deposition is required to prevent the diffusion between the solar cell layers.[13] However, it is still difficult to achieve high electrical conductivity and high transmittance simultaneously at RT for AZO films. It is suggested that the electrical properties of AZO thin films fabricated by magnetron sputtering at low deposition temperature are strongly affected by the deposition conditions and exhibit a resistivity inhomogeneity across the substrate.[14,15] The effect of off-center deposition on the optoelectronic properties of the AZO films fabricated by the magnetron sputtering method have been investigated.[16] However, to the best of our knowledge, the effect of both substrate rotation speed and off-axis deposition on the structural, optical, and electrical properties of AZO thin films grown by DC magnetron sputtering at RT is still lacking.

II. EXPERIMENTAL

A transparent conductive AZO layer was deposited onto soda-lime glass (SLG) substrates by DC magnetron sputtering from 2-in. ceramic targets of ZnO:Al_2O_3 [(98 wt. % ZnO and 2 wt. % Al_2O_3)] at RT. The target was pre-sputtered for 5 min. Deposition was performed with a DC power of 50 W and 50 sccm argon gas flow for 120 min. During the deposition, the working pressure was in the range from 3 to 5 mTorr. The vertical distance between the target and the substrate holder was 8 cm. The sample holder was rotated with different speeds around the center of the chamber by rotational feedthrough during the deposition to investigate the influence of substrate rotation speed. As shown in Fig. 1, SLGs were located onto the rotating sample holder both just above the target (position 0) and in off-center configurations (position 1 and 2) to investigate the effect of the horizontal distance between the target center and substrate on the properties of AZO films.

[a)]Author to whom correspondence should be addressed: fulyaturkoglu@iyte.edu.tr. Tel.: (+90) 232 750 7684. Fax: (+90) 232 750 7707.

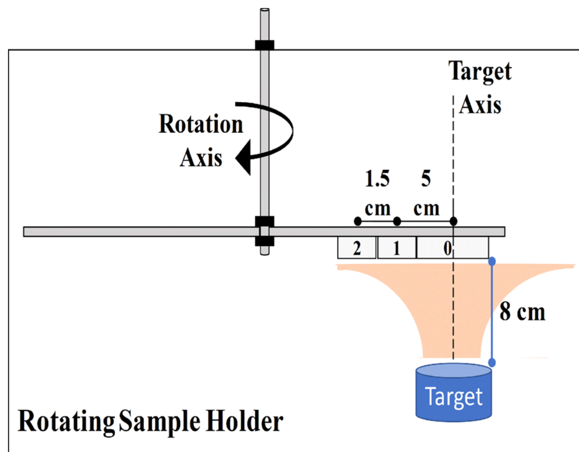

FIG. 1. Sample positions on the rotating sample holder.

To obtain information about the crystal structures of the AZO films, X-Ray Diffraction (XRD) was carried out in the Bragg-Brentano focusing geometry on a Phillips X'Pert Pro X-Ray diffractometer, with Cu Kα radiation ($\lambda = 1.5406$ Å). The XRD patterns were recorded from $2\theta = 20$–$80°$ with a step size of 0.016° for all samples. A Veeco DEKTAK 150 profilometer was used to determine the thicknesses of the films. The thicknesses of the films are given in Table I. The optical properties of the AZO films were investigated by transmittance measurements in the 200–2600 nm wavelength range using a PerkinElmer Lambda 950 UV/VIS/NIR spectrophotometer. Raman studies were performed using High-resolution Raman spectroscopy (Princeton Instruments, Acton SP2750 0.750 mm Imaging Triple Grating Monochromator) in the back-scattering mode with a spectral resolution of 1 cm^{-1} at room temperature. A wavelength of 488 nm Ion-Ar^+ was used with a 100 mW power. The electrical characteristics of AZO thin films were investigated to determine the sheet resistance of the films by the four-point probe technique using a Keithley 2420 source meter. The resistivity values of the films were obtained by multiplying the calibration constant (4.53), thickness, and sheet resistance of the films.

III. RESULTS AND DISCUSSION

A. XRD analyses

Crystallinity plays an important role in determining the optical and electrical properties of a thin film. Figure 2 shows the X-ray diffraction patterns of the AZO films deposited with different rotational speeds at different distances from the target axis. At all rotational speeds, the diffraction peak of AZO thin films appears at approximately 34.3 degrees which belongs to (002) reflection of the hexagonal wurtzite structure. This shows the formation of highly oriented grains along the c-axis due to self-texturing. We observed lower 2θ values for the AZO films with respect to bulk ZnO which has a diffraction line at 34.5. While there is a small shift in 2θ values for the AZO films placed in positions 1 and 2, for the AZO films placed on the 0 position, the 2θ shifts to more lower values and crystallinity deteriorates indicating a high degree of disorder.[17]

It is known that the (002) reflection peak of the AZO thin films shifts towards a lower or higher 2θ values with respect to bulk ZnO.[18] Al can substitute at the Zn sites or create oxygen vacancies after sitting as an interstitial atom. When Al is incorporated into the ZnO lattice, the AZO lattice is distorted due to the difference in the ion radius between Al^{3+} (0.039 nm) and Zn^{2+} (0.060 nm).[19] If the Al^{3+} ions substitute at the Zn^{2+} sites, the AZO crystal lattice constants are reduced. This leads to smaller interplanar spacing (d_s) and 2θ shifts to higher values according to Bragg's law. Moreover, Al can easily be interstitially solubilized in the ZnO octahedral site since the ratio of the atomic radius of Al to the atomic radius of ZnO $((r_{Al}/r_{ZnO}) = 1.180$ Å/1.625 Å $= 0.726)$ is lower than the maximum value for interstitial solubilization (0.732).[19] Since the AZO films grown at room temperature do not have sufficient activation energy for the Al to substitute at the Zn sites, many of Al^{3+} ion cations sit in the films as an interstitial ion which leads to higher interplanar spacing.[19,20] The variation of the 2θ values and interplanar spacing derived from the (002) peak position can be seen in Table I. For all films, d_s values are larger than that of bulk ZnO which is equal to 0.2603 nm which indicates that all the films exhibit compressive stresses and the stress

TABLE I. Variation of the thickness, deposition rate, (002) peak positions, d spacing, strain, stress, resistivity, and energy gap values of AZO thin films with different positions on the sample holder and rotation speed.

Rotation speed (rpm)	Sample position	Target to substrate distance (cm)	Thickness (nm)	Deposition rate (nm/min)	2θ	d spacing (Å)	Strain	Stress (GPa)	Resistivity (10^{-3} Ω cm)	Eg (eV)
0.0	0	0.0	600	6.67	33.76	2.66	0.0191	4.27	272	3.185
0.0	1	5.0	450	5.00	34.20	2.62	0.0065	1.44	5.30	3.410
0.0	2	6.5	250	2.78	34.31	2.61	0.0033	0.73	4.47	3.682
3.3	0	0.0	230	2.56	33.70	2.66	0.0209	4.66	208	3.317
3.3	1	5.0	182	2.02	34.32	2.61	0.0029	0.65	3.13	3.620
3.3	2	6.5	142	1.58	34.36	2.61	0.0018	0.39	3.02	3.721
6.3	0	0.0	190	1.58	33.71	2.66	0.0207	4.63	55.90	3.356
6.3	1	5.0	165	1.38	34.31	2.61	0.0034	0.75	3.06	3.647
6.3	2	6.5	135	1.13	34.36	2.61	0.00210	0.47	2.02	3.745
12.0	0	0.0	218	2.42	33.78	2.65	0.0185	4.13	198	3.317
12.0	1	5.0	172	1.91	34.32	2.61	0.0030	0.67	4.30	3.570
12.0	2	6.5	123	1.37	34.38	2.61	0.0012	0.26	4.12	3.768

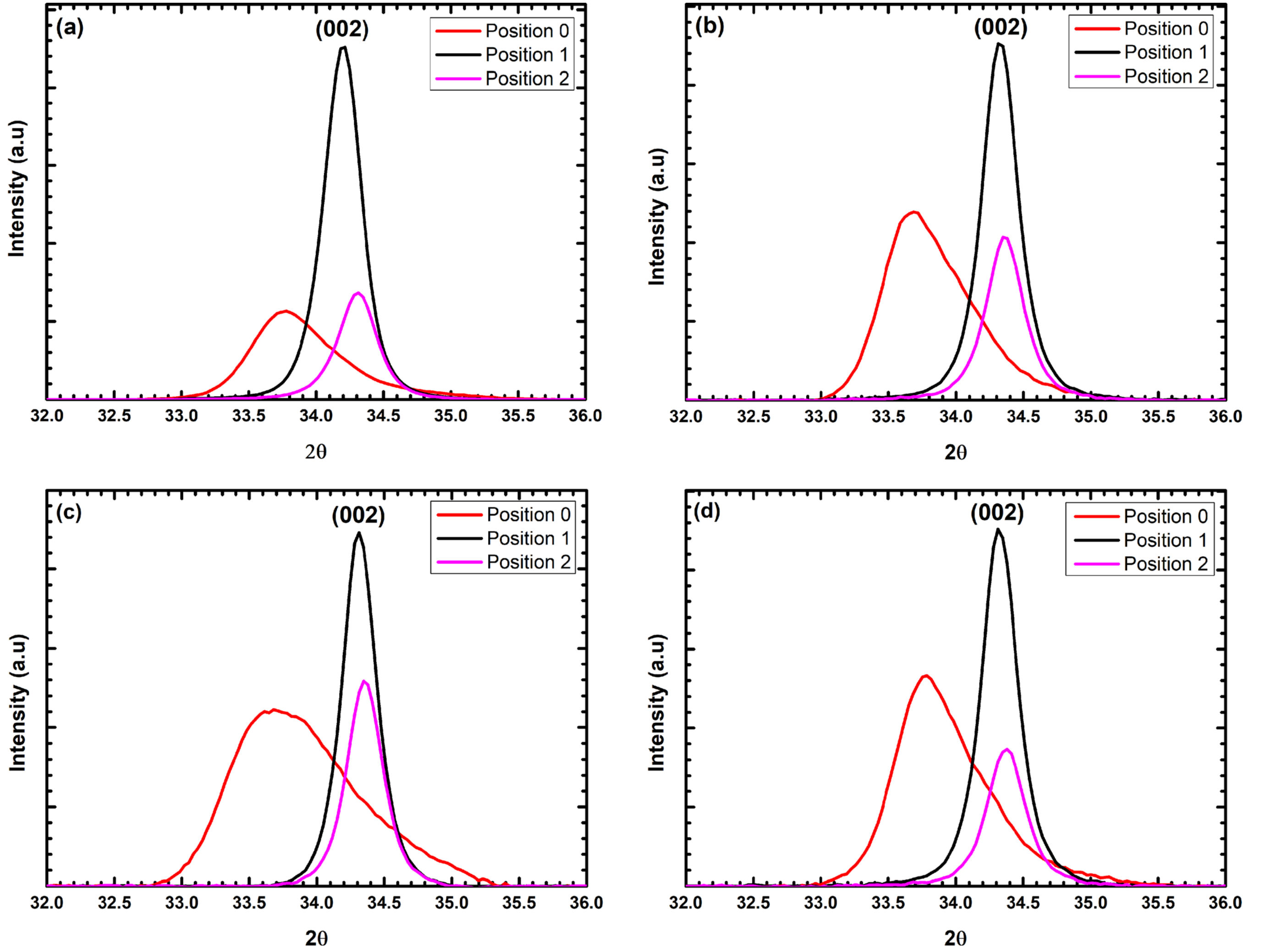

FIG. 2. X-ray diffraction patterns of AZO films deposited with (a) 0 rpm, (b) 3.3 rpm, (c) 6.3 rpm, and (d) 12 rpm rotating speeds at different distances from the target axis.

is caused predominantly by the interstitial Al^{3+}. Moreover, as the distance between the substrate and the target axis increased, the shift in 2θ values decreases.

The oxygen atoms at the surface of the AZO target are ionized and accelerate towards the substrate during the sputtering. These negative oxygen ions are neutralized during their transits. However, they can reach the substrate with sufficient energy to be implanted. When the sample is placed away from the target, sputtered particles and argon ions collide frequently, and their energy is reduced while traveling to the substrate. Therefore, direct bombardment of the high energetic negative ions is significantly reduced by the off-center configuration. When the sample placed in front of the target, the energetic sputtered particles arrive at the substrate with high kinetic energy due to decrement in the number of collisions between sputtered particles and argon ions.[19] The high energetic oxygen ion bombardments produce more defect like inter-stresses[21] Furthermore, direct bombardment of high energetic O atoms on the surface may possibly combine with Al atoms to form aluminum oxides and limit the doping effect.[21,22] Formation of these defects and phases leads to a more compressive stress in the film.

The total residual stress in the thin films consists of the intrinsic stress induced by the doping and defects during the fabrication process and, the extrinsic stress induced by different lattice constants and thermal expansion coefficients of the thin film and its substrate.[23] Since no heat treatment was applied to the films during sputtering, the differences in the residual stress of our AZO films is mainly intrinsic stress resulting from growth conditions.

The stress in the films can be estimated using the following formula, which is valid for a hexagonal lattice

$$\sigma_{film}^{XRD} = \frac{2c_{13}^2 - c_{33}(c_{11}+c_{12})}{2c_{13}} * \frac{c_{film} - c_{bulk}}{c_{bulk}}, \quad (1)$$

where c_{ij} is the elastic stiffness constant of single crystalline ZnO ($c_{11} = 208.8$, $c_{33} = 213.8$, $c_{12} = 119.7$, and $c_{13} = 104.2$ GPa).[24] c_{film} and c_{bulk} are the lattice constants of the AZO films and bulk ZnO thin films, respectively. This yields the numerical relation between the in-plane stress and out-plane strain, $\sigma_{film} = 223*\varepsilon$ (GPa). The strains in the films were derived using the relation $((d_s\text{-}d_0)/d_0)$, where d_0 is the inter-planar spacing of bulk ZnO. The estimated strain and stress values of the AZO films are shown in Table I. Positive

values of strains indicate the tensile strain and negative values of stresses indicate the compressive stress in our AZO films. Figure 3 shows how the position of the substrate and rotation speeds affect the stress in the films. According to this figure, the stress in the films decreases when the substrate position with respect to the target axis increases. Moreover, we observed small reduction of the stress in the films with increasing rotation speed. As given in Table I, the deposition rate for stationary samples is much higher than the deposition rate for rotating samples. According to deposition rates, when the substrate is rotating, the duration of the substrate residence in front of the target decreases. Therefore, sputtered particles and argon ions collide more frequently with increasing rotation speed, and the energy of sputtered species is reduced before reaching the substrate. Stationary samples are more exposed to direct bombardment of high energetic negative ions due to the high energy of sputtered species. From these findings, the bombardment of highly energetic negative ions on the surface can be concluded and so stress in the films can be significantly reduced by off-center deposition and rotating the substrate during the deposition.

B. Raman analyses

Since Raman scattering by the phonons is determined by the electrons that remote the scatter phenomenon, Raman spectra contain information not only about phonons but also about electrons and electron-phonon interactions.[25] Therefore, Raman measurements were performed to better understand the correlation between the structural and electrical properties of the AZO films. Figure 4 shows the Raman spectra of AZO films excited at 488 nm. Raman spectra consist of two Raman active modes around 446 and 582 cm^{-1}. The Raman modes at 800 cm^{-1} are due to the SLG substrate. The observed Raman modes are assigned as follows. The peak at 446 cm^{-1} is the E_2 (High) mode of ZnO associated with the wurtzite structure and is related to vibration of only oxygen atoms.[26] It is worth noting that the E_2 (High) mode shifts higher frequencies (blue shift) for all samples, which is generally observed around 437–444 cm^{-1}. E_2 (High) phonon frequency is affected by stresses in the wurtzite structure or

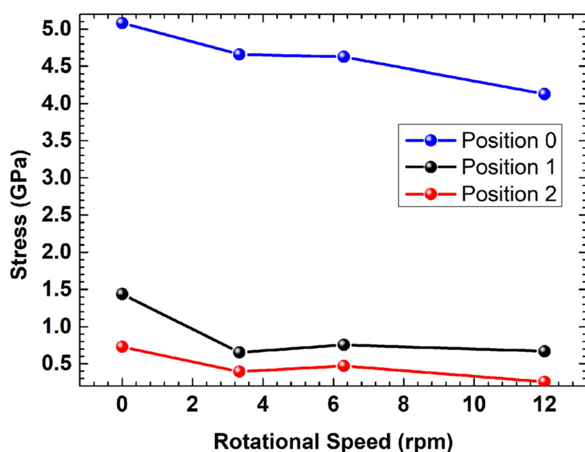

FIG. 3. Effect of position of the substrate and rotation speed on the stress in the films.

laser induce heating.[27,28] The blue shift in the E_2 (High) is attributed to compressive stress, whereas the red shift in the E_2 (High) is attributed to tensile stress. However, the peak position of the E_2 (high) mode remains the same for all AZO films even for the samples in position 0. Thus, we attributed observed a blue shift to local heating induced by UV laser. The vibration line around 582 cm^{-1} corresponds to the E_1 (LO) mode of ZnO, which is very sensitive to the oxygen deficiency and free carrier.[29–31] Strong coupling of the free carrier with the E_1 (LO) mode would cause a red shift.[31] We observed that the position of the E_1 (LO) mode strongly depends on the position of the sample and rotation speed. For distant samples, this peak shift to lower values regardless of the rotation speed and as the distance between the substrate and target axis increased, the amount of shift increases. Also, as it can be seen when the substrate is rotated during deposition, the amount of shift is higher with respect to non-rotating substrates. Increase in the red shift of the E_1 (LO) vibration line indicates the enhancement in oxygen vacancies in our samples as the horizontal distance between the substrate and target axis is increased and/or substrate is rotated. We may also attribute this shift to the increasing carrier concentration of the films since the sheet resistance of AZO thin films fabricated at room temperature strongly related to the amount of oxygen vacancies.[30] The oxygen vacancies create maximum two free electrons per vacancy to the donor level through ionization, leading to an increase in conductivity. A quantitative comparison of the peak intensities may not be meaningful due to different thicknesses of the films.

C. Transmission analysis

Figure 5 illustrates the transmittance spectra of our AZO films. As can be seen, the average transmittance of all AZO films in the visible region (400–800 nm range) exceeds 85% which is important for applications in the field of solar cells. The absorption edge of the samples (sharp decrease in transmittivity) was observed in the range from 300 to 400 nm. We observed that the absorption edge shifts to shorter wave lengths as the distance between the substrate and target axis increased. This blue shift can be attributed to an increase in the band gap energy resulting from the Burstein-Moss effect which is related to the carrier concentration. That is, with increasing distance between the substrate and target axis, the optical band gap of the films grows due to increased carrier concentration and causes the absorption edge to shift to short wave lengths. Moreover, we observed that transmission of the samples located in off-center configurations (positions 1 and 2) is lower than the samples located above the target (position 0) in the infrared region. The concentration of free carriers is important for the optical transmission of AZO films in the near infrared region. A high free carrier concentration causes high reflection or lower transmission of the infrared region.[32]

The Tauc method was used to calculate the energy gap of the samples to better understand the blue shift of the absorption edge. In the present study, the absorption coefficient, α^2 versus photon energy ($h\nu$) plot was used to estimate the bandgap

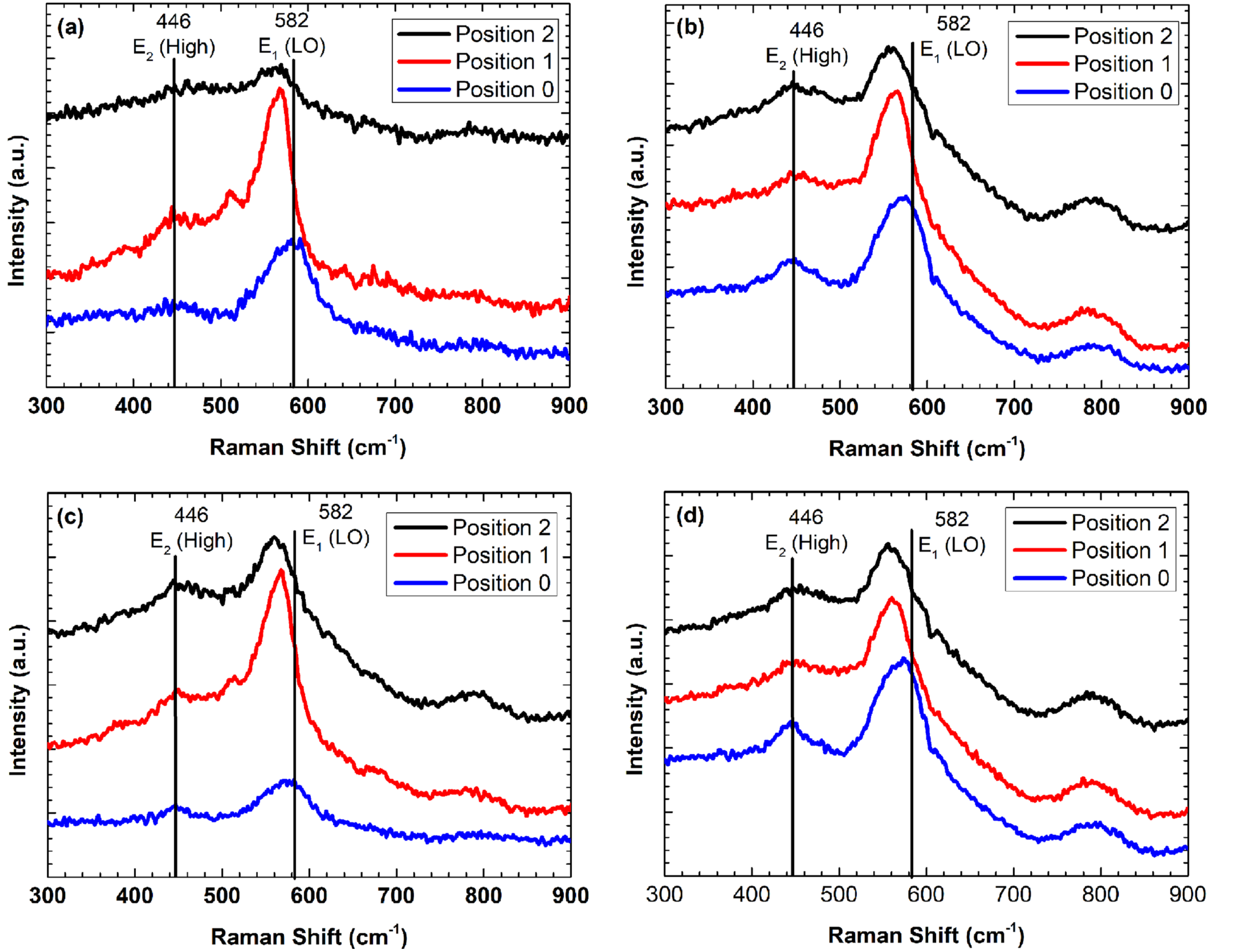

FIG. 4. Raman spectra of AZO films deposited at (a) 0 rpm, (b) 3.3 rpm, (c) 6.3 rpm, and (d) 12 rpm.

energy of the AZO thin films (Fig. 6). Absorption was calculated by the equation

$$T - R = e^{-\alpha t}, \tag{2}$$

where T and R denote the transmittance and reflectance, respectively, and t is the thickness of the film. The reflectance of the films was neglected due to its relatively low value,[31] and then the absorption coefficient was simplified as

$$\alpha^2 = (lnT)^2/t^2. \tag{3}$$

Since aluminum doped zinc oxide has a direct transition, i.e.,

$$\alpha h\nu = A(h\nu - E_g)^{1/2}, \tag{4}$$

the bandgaps of the films are deduced from the extrapolation of the linear plots of α^2 versus hν.

Figure 6 shows the α^2 vs photon energy graph of AZO films coated at different rpm and at different distances from the target axis. The change in the energy band gap of AZO films deposited at different rpm and at different distances from the target axis is clearly visible in Fig. 7(a). We observed that the optical energy gap shifts towards higher energies for the samples deposited at larger distances from the target axis (in a position sequence 0–2) regardless of the rotating speed. As mentioned before, increase in the energy band gap can be interpreted by the Burstein-Moss effect results from the Pauli Exclusion Principle. Donor electrons due to Al or oxygen vacancies normally occupy the higher energy levels in the conduction band. As a result, the effective band gap (E_g) of an AZO film should be relatively higher when compared to the separation in energy between the top of the valence band and the unoccupied energy states in the conduction band of this direct band gap semiconductor. Consequently, band gap moves to higher energy. The widening in the band gap (Burstein–Moss shift) is dependent on the carrier concentration, n, according to $n^{2/3}$. The reason for the low band gap of the samples in position 0 is to have low carrier concentrations due to high compressive stress, as the stress relaxes for the samples in position 1 and 2 carrier concentrations and so the band gap of the samples increases. Moreover, as the sample holder rotational speed increases, the band gap increases regardless of the sample position indicating increase in carrier concentrations. On the other hand,

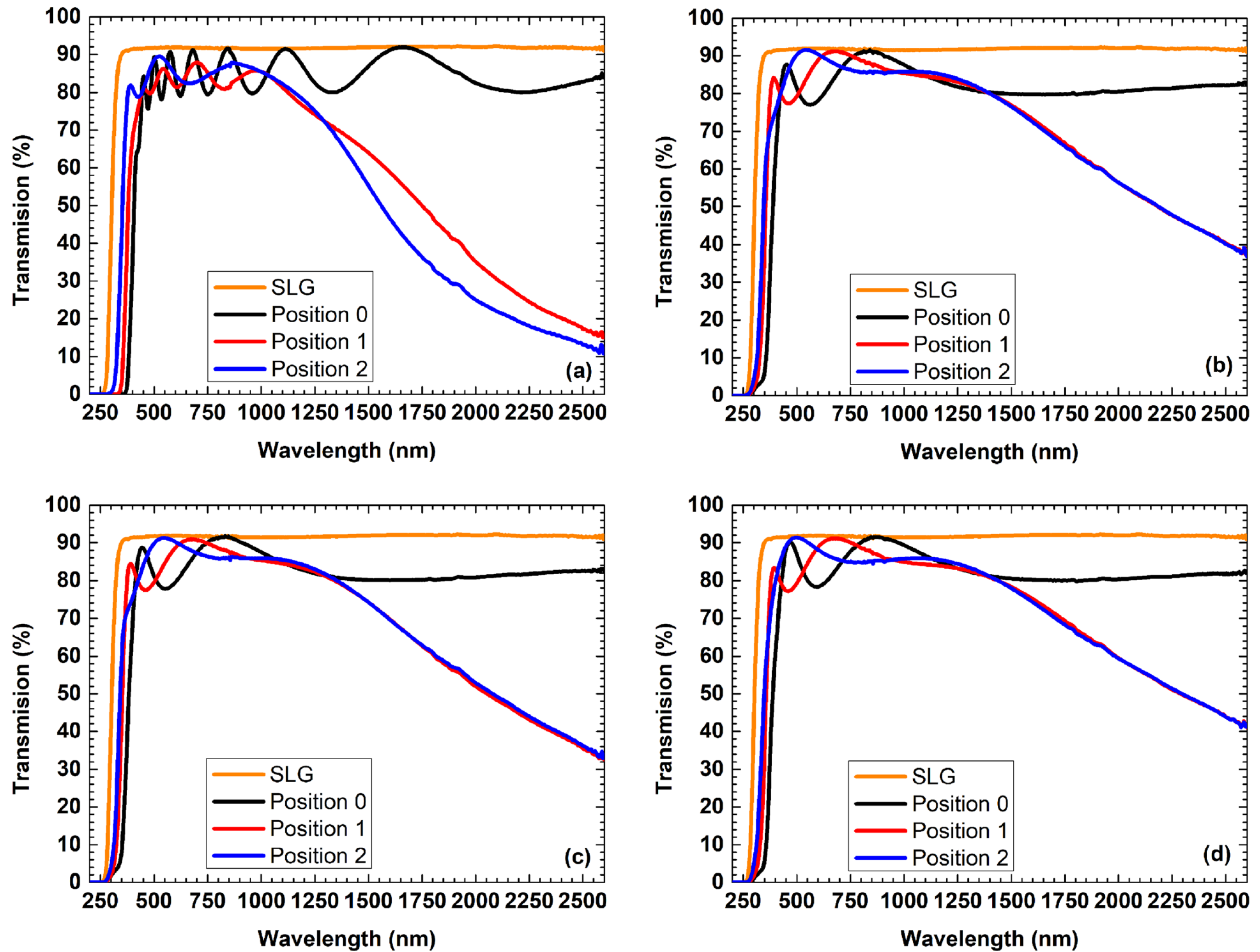

FIG. 5. Transmittance spectra of AZO films deposited at (a) 0 rpm, (b) 3.3 rpm, (c) 6.3 rpm, and (d) 12 rpm.

it is further observed a small decrease in band gap occurs for a high rotation speed (12.0 rpm). Such a red-shift of the optical band gap of AZO thin films has been explained in terms of relaxation of in-plane stress by Mohanty *et al.*[33] According to their observation, the positive shift in E_g is well predicted by the BM effect for moderate values of carrier concentrations up to the Mott critical density. For higher carrier concentrations above the Mott critical density, the BM effect is compensated by band gap shrinkage. Shallow level donor and shallow level acceptor impurities create energy levels in the band gap near the conduction band edge and the valence band edge, respectively. At high carrier concentrations, the density of states of these dopants increase and forms a continuum of states like in the bands and the effective band gap of AZO is narrowed. From these observations, we conclude that the carrier concentration of the films increases for off-center configurations and rotating samples during deposition since defects induced by the bombardment of high energetic negative ions are significantly reduced for these samples.

D. Electrical properties of AZO thin films

The electrical property of AZO films is also an important factor for its performance in devices. Figure 7(b) shows the resistivity values measured by the four-point method versus the sample holder rotation speed for AZO thin films coated at positions 1 and 2. The films in position 0 have not been investigated because their resistivity values are very high. According to the XRD, strong enhancement of the resistivity for the substrate position facing the target is due to the high compressive stress in the films. Raman spectroscopy and Transmission measurements also indicate the low carrier concentrations for the films in position 0. For the off-center configurations, lower resistivity of AZO thin films can be correlated to the amount of donors, mainly oxygen vacancies and Al interstitial atoms which supply conduction electrons from donor sites. It has been observed that the resistivity of the films in position 2 is lower than those in position 1 regardless of the rotation speed. This behavior attributed to higher carrier concentrations for the films in position 2, and this attribution seems consistent with the XRD, Raman, and Transmission data. We further observed that as the sample holder rotation speed increases, resistivity decreases regardless of the sample position. On the other hand, a small increase in resistance at 12.0 rpm may be attributed to the likelihood of higher carrier concentration. The lowest resistivity value was found to be 2.02×10^{-3} Ω cm for the AZO film in position 2 rotating at 6.3 rpm. As seen in Fig. 7, the change observed in the band

FIG. 6. Tauc plots of AZO films deposited at (a) 0 rpm, (b) 3.3 rpm, (c) 6.3 rpm, and (d) 12 rpm.

gap of the AZO films is in a perfect agreement with the charge carrier properties, as the band gap of the samples increases, the resistivity values of the films decreases due to the increment of carrier density in films.

E. Conclusion

In this work, we investigate the effect of both substrate rotation speed and off-axis deposition on the optical and electrical properties of AZO thin films grown by DC magnetron

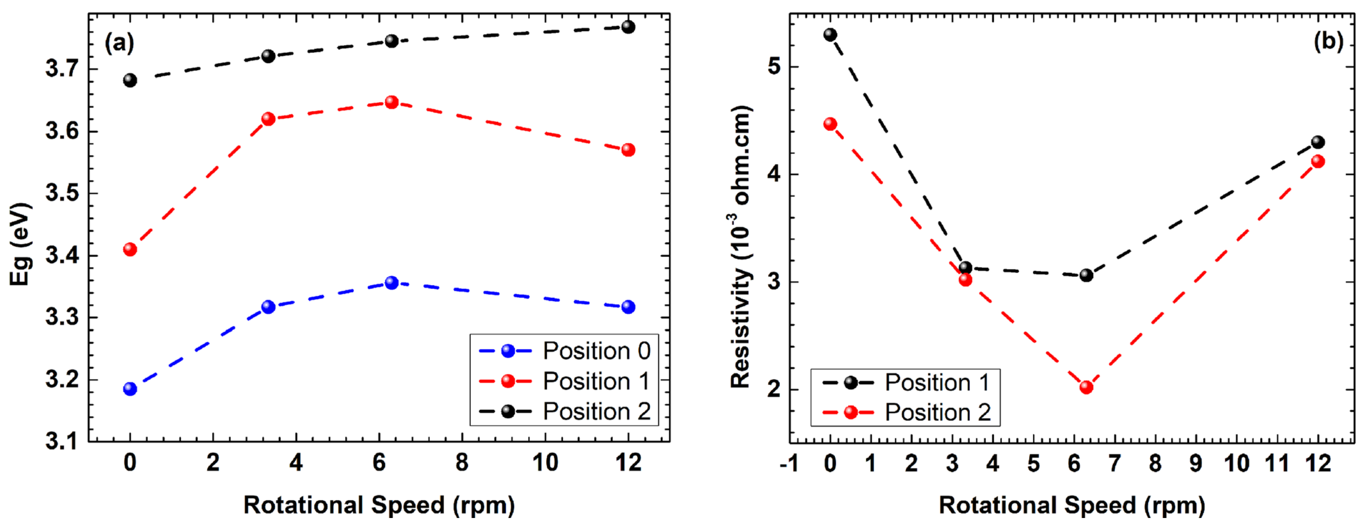

FIG. 7. (a) Energy gap values versus the sample holder rotation speed for AZO thin films at different positions on the sample holder and (b) resistivity values measured by the four-point method versus the sample holder rotation speed for AZO thin films coated at positions 1 and 2.

sputtering at RT. XRD, Raman, and Transmission measurements revealed the correlation between the structural, optical, and electrical properties of the AZO films depending on the growth conditions. We demonstrate that the crystallinity and resistivity of the AZO films fabricated at RT can be improved by both off-center deposition and rotating the sample holder during sputtering. An average transmittance above 85% in the visible range (400–800 nm) and a resistivity of 2.02×10^{-3} Ω cm were obtained for the AZO films deposited at 6.5 cm away from the target axis and rotating at 6.3 rpm. Since RT deposition of AZO thin films prevents the diffusion between the solar cell layers, the results presented here may help us to achieve thin film solar cells with higher efficiencies.

ACKNOWLEDGMENTS

This research was supported in part by the TUBITAK (Scientific and Technical Research Council of Turkey) Project No. 114F341 and the authors would like to acknowledge the facilities of the Applied Quantum Research Center (AQuReC) for the current study.

[1]D. S. Ginley, H. Hosono, and D. C. Paine, *Handbook of Transparent Conductors* (Springer Science and Business Media, New York, 2010).
[2]O. Tuna, Y. Selamet, G. Aygun, and L. Ozyuzer, J. Phys. D: Appl. Phys. **43**, 055402 (2010).
[3]D. Johnston, Sol. Energy **84**(3), 384–389 (2010).
[4]R. G. Gordon, MRS Bull. **25**(08), 52–57 (2000).
[5]K. Ellmer, A. Klein, and B. Rech, *Transparent Conductive Zinc Oxide: Basics and Applications in Thin Film Solar Cells* (Springer, New York, 2008).
[6]Y. Liu, Y. Li, and H. Zeng, J. Nanomaterials **2013**, 196521.
[7]T. Minami, Semicond. Sci. Technol. **20**, 35–44 (2005).
[8]S. L. Ou, D. S. Wuu, S. P. Liu, Y. C. Fu, S. C. Huang, and R. H. Horng, Opt. Express **19**, 16244–16251 (2011).
[9]T. Terasako, M. Yagi, M. Ishizaki, Y. Senda, H. Matsuura, and S. Shirakata, Surf. Coat. Technol. **201**(22), 8924–8930 (2007).
[10]G. Paul, R. Ghosh, S. Bera, S. Bandyopadhyay, T. Sakurai, and K. Akimoto, Chem. Phys. Lett. **463**(1), 117–120 (2008).
[11]M. Kumar, R. Singh, S. Nandy, A. Ghosh, S. Rath, and T. Som, J. Appl. Phys. **120**, 015302 (2016).
[12]K. Ellmer, J. Phys. D: Appl. Phys. **33**, R17 (2000).
[13]C. S. Ferekides, D. Marinskiy, V. Viswanathan, B. Tetali, V. Palekis, P. Selvaraj, and D. Morel, Thin Solid Films **361**, 520–526 (2000).
[14]X. B. Zhang, Z. L. Pei, J. Gong, and C. Sun, J. Appl. Phys. **101**, 014910 (2007).
[15]A. Bikowski, T. Welzel, and K. Ellmer, J. Appl. Phys. **114**, 223716 (2013).
[16]S. Ou, F. Lai, L. Yuan, D. Cheng, and K. Kao, J. Nanomaterials **2016**, 6250640.
[17]P. Gondoni, M. Ghidelli, F. Di Fonzo, V. Russo, P. Bruno, J. Martí-Rujas, C. E. Bottani, A. Li Bassi, and C. S. Casari, Thin Solid Films **520**(14), 4707–4711 (2012).
[18]R. C. R. Nagiri, S. D. Yambem, Q. Lin, P. L. Burn, and P. Meredith, J. Mater. Chem. C **3**(20), 5322–5331 (2015).
[19]H. C. Nguyen, T. T. Trinh, T. Le, C. V. Tran, T. Tran, H. Park, V. Dao, and J. Yi, Semicond. Sci. Technol. **26**(10), 105022 (2011).
[20]H. Wang, J. Xu, M. Ren, and L. Yang, J. Mater. Sci.: Mater. Electron. **19**(11), 1135–1139 (2008).
[21]H. Zhu, J. Hüpkes, E. Bunte, and S. M. Huang, Appl. Surf. Sci. **256**(14), 4601–4605 (2010).
[22]D. Horwat and A. Billard, Thin Solid Films **515**(13), 5444–5448 (2007).
[23]M. S. Kim, K. G. Yim, J. S. Son, and J. Y. Leem, Bull. Korean Chem. Soc. **33**(4), 1235–1241 (2012).
[24]R. Cebulla, R. Wendt, and K. Ellmer, J. Appl. Phys. **83**(2), 1087–1095 (1998).
[25]V. Russo, M. Ghidelli, P. Gondoni, C. Casari, and A. Li Bassi, J. Appl. Phys. **115**(7), 073508 (2014).
[26]Ü. Özgür, Y. I. Alivov, C. Liu, A. Teke, M. Reshchikov, S. Doğan, V. Avrutin, S. J. Cho, and H. A. Morkoc, J. Appl. Phys. **98**(4), 041301 (2005).
[27]K. A. Alim, V. A. Fonoberov, M. Shamsa, and A. A. Balandin, J. Appl. Phys. **97**(12), 124313 (2005).
[28]S. B. Yahia, L. Znaidi, A. Kanaev, and J. Petitet, Spectrochim. Acta Part A **71**(4), 1234–1238 (2008).
[29]N. Srinatha, Y. No, V. B. Kamble, S. Chakravarty, N. Suriyamurthy, B. Angadi, A. M. Umarji, and W. Choi, RSC Adv. **6**(12), 9779–9788 (2016).
[30]X. Xu, S. Lau, J. Chen, G. Chen, and B. Tay, J. Crystal Growth **223**(1), 201–205 (2001).
[31]J. N. Zeng, J. K. Low, Z. M. Ren, T. Liew, and Y. F. Lu, Appl. Surf. Sci. **197**, 362–367 (2002).
[32]H. Koseoglu, F. Turkoglu, M. D. Yaman, M. Kurt, F. G. Akça, G. Aygun, and L. Ozyuzer, Vacuum **120**, 8–13 (2015).
[33]B. C. Mohanty, Y. H. Jo, D. H. Yeon, I. J. Choi, and Y. S. Cho, Appl. Phys. Lett. **95**, 062103 (2009).